RSC Advances

ROYAL SOCIETY OF CHEMISTRY

www.rsc.org/advances

Journal Name

ARTICLE

One-step synthesis of magnetic gold nanostars for bioimaging applications

Received 00th January 20xx,
Accepted 00th January 20xx

DOI: 10.1039/x0xx00000x

www.rsc.org/

L. Minati[a*†], V. Antonini[b], L. Dalbosco[c], F. Benetti[c], C. Migliaresi[c], M. Dalla Serra[b], G. Speranza[a]

This work presents novel magnetite-gold hybrid nanoparticles formed by multiple magnetic cores inside gold nanostars (SPIO@Au). The nanostructures were produced by one-step hydroxylamine reduction of gold precursor on the surface of functionalized superparamagnetic iron oxide nanoparticles in aqueous alkaline medium. The nanoparticles show excellent chemical stability, magnetic properties and an intense surface plasmon resonance in the visible-NIR region. *In vitro* cellular tests showed that these nanostructures could be efficiently internalized inside A549 cells. The optical properties of the SPIO@Au nanoparticles were exploited for *in vitro* localization analysis through scattering based imaging. These nanoparticles could have enormous potential for applications as contrast agent in combined imaging techniques as well as in bio-analytical applications such as biomolecule and cells separation.

Introduction

The development of nanoparticles with multiple functionalities has become of considerable interest in biomedicine.[1-3] Multifunctional nanoparticles give the possibility to develop new combined imaging approaches that can overcome the intrinsic limitations of the individual techniques.[4, 5] In the last years superparamagnetic iron oxide NPs have been extensively used as contrast agent in magnetic resonance imaging because of their high performance in T_2 weighted magnetic resonance imaging (MRI).[6, 7] However, one of the most important MRI drawbacks is its limited spatial resolution.[8] On the contrary, optical based techniques as photoacoustic tomography or two-photon luminescence provide high spatial resolution analysis. Unfortunately, the penetration depth of the electromagnetic radiation (typically in the NIR range) into the living tissue is limited to several millimeters.[9] Because of the above considerations, nanoparticles with multiple functionalities can have a great interest as contrast agents for many applications in medicine. Magnetic-plasmonic nanoparticles composed by an iron oxide core and a gold shell are the best candidates for multimodal imaging applications.[10] The production of spherical core-shell nanoparticles with compact dimension (lower than 50 nm) is beneficial for the biodistibution and circulation in the blood system, but these nanoparticles show poor extinction in the red-NIR range[11]. This is a consequence of the small thickness of the gold coating surrounding the magnetic core. One of the possible solutions to boost the optical properties of the core shell nanoparticles in the red-NIR range involves the formation of an anisotropic non-spherical metallic shell. Anisotropic gold nanoparticles as gold nanostars have an increased absorption in the red-NIR range compare to the traditional spheroidal nanoparticles. In addition, for these particular geometries, the surface plasmon resonance (SPR) peak of gold shifts to the NIR region (650 and 800 nm).[12] The combination of iron oxide core magnetic properties, chemical stability and superior optical properties of the gold nanostars is expected to open new opportunities in imaging and therapy, with particular emphasis in combined imaging techniques able to overcome the limitation of the individual technique. One of the examples in this field is the magneto-photo-acoustic imaging developed by Emilianov et al. [13] as well as magnetomotive imaging reported by Wei et al.[14] In recent years several synthesis procedure were developed to produce magnetic gold nanostars.[15, 16] Most of these procedures required multiple steps process to coat the magnetic nanoparticles with the gold shell. The multi-step approach complicates the synthesis procedure in particular for the mass production of these nanoparticles. In this work, magnetic gold nanostars were synthesized by controlled reduction of gold chloride on the surface of polyethylene glycol (PEG) functionalized 10 nm superparamagnetic iron oxide nanoparticles. The gold reduction was obtained in one single step process in strong basic environment in presence of hydroxylamine. The resulting nanostructures are composed by multiple magnetic nanoparticle cores embedded into star shaped gold nanoparticles. This procedure significantly decreases the overall synthesis time compared to the classical seed-

[a] *FBK, Via Sommarive 18, 38123 Trento, Italy*
[b] *Istituto di Biofisica, Consiglio Nazionale delle Ricerche, via alla Cascata 56/C, 38123 Trento, Italy*
[c] *Department of Industrial Engineering & Biotech Research Center, University of Trento, via delle Regole 101, 38123 Mattarello, Trento*
† Present address: Istituto di Biofisica, Consiglio Nazionale delle Ricerche via alla Cascata 56/C, 38123 Trento, Italy
Electronic Supplementary Information (ESI) available: Additional XPS, EDS, TEM and confocal microscopy images are presented. See DOI: 10.1039/x0xx00000x

growth method. The small size of the nanoparticles were achieved by controlling the gold to iron molar ratio and by fine-tuning the optimal pH of the reaction. The as-prepared SPIO@Au NPs showed superior magnetic properties and an efficient absorption of the light in the NIR range. SPIO@Au nanoparticles were functionalized with anti-fouling, biocompatible thiol-functionalized PEG for their application as *in vitro* optical contrast agent. Laser Scanning Confocal Microscopy (LSCM) analysis revealed that SPIO@Au can effectively penetrate the plasma membrane of A549 cancer cells. The optical properties of the SPIO@Au were exploited for the nanoparticles localization inside A549 cancer cell through scattering based imaging without the need of further functionalization with fluorescent tags.

Experimental

Materials. Tetrachloroauric acid ($HAuCl_4$), hydroxylamine, iron oxide nanoparticles and polyethylene glycol methyl ether thiol were purchased from Sigma (Milwaukee, WI, USA).
1,2-distearoyl-*sn*-glycero-3-phosphoethanolamine-N [amino (PEG)-2000] (DSPE-PEG-amine) and 1,2 distearoyl-sn-glycero-3-phosphoethanolamine-N-[methoxy (PEG)-2000] (DSPE-PEG) and were purchased from Avanti Polar Lipid, inc.

Synthesis of SPIO-PEG nanoparticles. A suspension of iron oxide nanoparticles (SPIO) coated by oleic acid in toluene (3 ml, 1 mg / ml) was added to 5 ml of chloroform under mixing.
A solution of DSPE-PEG (4.5 ml, 5 mg/ml) and DSPE-PEG-amine (240µl, 5 mg/ml) in chloroform were added to the suspension under mixing obtaining a homogeneous mixture. After stirring, the mixture was dried with argon and left in vacuum for 48 hours in order to remove all traces of organic solvents.
The dried film was suspended again in Milli-Q water by ultrasonication for 30 minutes.
The excess lipids were removed from the suspension by repeated ultracentrifugation (25,000 rpm for 1h, 3 times).

Synthesis of SPIO@Au nanoparticles. The purified nanoparticles (10 µg) were dissolved in 0.45 ml aqueous solution at pH 12 by NaOH. After 1 minute incubation with continuous stirring, 50 µl of 10mM $HAuCl_4$ aqueous solution (total Au^{3+} concentration in the solution 1mM) were added and the suspension was stirred for 5 other minutes. The reducing agent NH_2OH (200 mM in H_2O, 50 µL) was then introduced into the solution in order to start gold precursor reduction. The solution color changes from pale yellow to green blue in less than 1 minute. The nanoparticles were purified by a series of centrifugation (10000 rpm for 10 minutes) and magnetic separation using a commercial magnet.

Synthesis of SPIO@Au-PEG. SPIO@Au were further functionalized with poly(ethylene glycol) methyl ether thiol (PEG, Mn 5000 Da) by dissolving 50 µg of SPIO@Au in a 1 mg/ml PEG-SH water solution under stirring for 12 h. The suspension was purified by centrifugation at 12000 rpm and magnetic separation. This procedure was repeated three times.

Cell uptake of SPIO@Au-PEG nanoparticles. Typically, 45000 A549 cells were seeded onto 16-mm glass coverslips in a 24-well plate and allowed to grow for 1 day at 80 % confluence. Then the medium was replaced by 500 µl of fresh culture medium supplemented with 25mM Hepes with SPIO@Au nanoparticles (0.05 mg/ml). The supernatant was left for 2 hrs. Before being analyzed by confocal microscopy (Leica 200D microscope equipped with an argon laser source), cells were washed three times with DPBS (Dulbecco`s Phosphate buffered saline).

Characterization. UV-vis absorption measurements were performed using an UV–visible–near infrared spectrophotometer (Cary 5000) in dual beam mode. For TEM analysis, the colloidal suspensions were deposited and dried onto a carbon-coated copper grid. Samples were observed using a Philips CM12 TEM operated at 120 kV and equipped with an energy dispersive X-ray spectrometer. Scanning Electron Microscopy analysis was carried out in a JSM-7001F instrument equipped with a thermal field emission gun. Images were acquired with samples placed at 90° with respect to the analyzer direction. Particle sizes were determined by dynamic light scattering (DLS) in back scattering mode at 25°C, using a laser particle sizer (Malvern Zetasizer Nano ZS, equipped with a He–Ne laser at 633 nm, 5 mW). In this assay, particle samples were diluted in milli-Q water to a final concentration of 0.01 mg/ml. Data were analyzed by the Malvern Proprietary Software. The obtained distributions were expressed as number-weighted size distribution. XPS measurements were performed using an ESCA200 instrument (Scienta-Gammadata ESCA 200 Uppsala Sweden). Wide scans were acquired in the binding energy (BE) range 1200 – 0 eV. Laser scanning confocal microscopy (LSCM) analysis was carried out using a Leica 200D microscope equipped with an argon laser source. For SPIO@Au localization analysis A549 cells membrane have been stained for 10 min with WGA-AlexaFluor 488 and then analyzed by confocal microscopy (excitation 488 nm, emission 520 nm). SPIO@Au localization was analyzed by exciting at 633 nm and acquiring in the range 620-650 nm.

Results and discussion

Fig. 1 schematically illustrates the synthesis of the SPIO@Au NPs. Highly monodispersed SPIO capped with oleic acid, were first solubilized into an aqueous solution using a mixture of phospholipid-polyethylene glycol and phospholipid-polyethylene glycol terminated with amine group. This procedure is a variation of the process described by Dubertret et al. [17] The hydrophobic phospholipid segment interpenetrate the oleic acids tails through hydrophobic interactions, whereas the PEG block facing outwards renders the SPIO NPs water-soluble and positively charged because of the terminal amino groups. In Fig. S1 the XPS analysis of the SPIO-PEG NPs is reported. The C1s core line show the presence of CH sp^3 carbon associated to the hydrophobic tail of the polymer and the oleic acid chains present on the surface of the iron oxide nanoparticles. The peak at 286 eV is associated to the C-O bonds of the PEG chains.[18] The analysis revealed also the presence of C-N bonds of the amino groups on the DSPE-PEG-amine. The presence of the PEG section allows to effectively stabilizing the nanoparticles in aqueous solution, even under strongly basic condition used for the reduction of the gold precursor (pH 12).

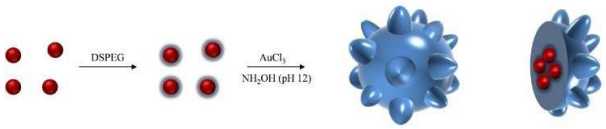

Fig. 1. Scheme of the SPIO@Au nanoparticle synthesis.

For SPIO@Au NPs synthesis, a volume of $HAuCl_4$ aqueous solution was added to SPIO–PEG suspension (pH adjusted to 12) and incubated for 5 min. The reducing agent hydroxylamine was then introduced to start gold reduction. During the reaction, the suspension color changed from pale yellow to dark green-blue in less than a minute (Fig. S2).

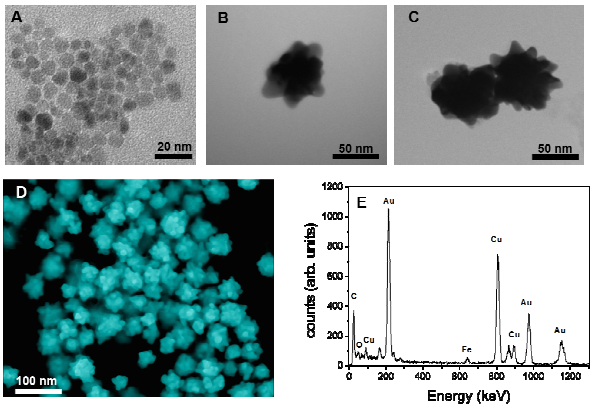

Fig. 2. A Transmission electron microscopy images of the SPIO nanoparticles. **B, C** TEM images of the SPIO@Au nanoparticles **D** False-colour scanning electron microscopy of the SPIO@Au nanoparticles. **E** EDXS analysis of SPIO@Au nanoparticles. Cu peaks comes from the copper grid.

The transmission electron microscope images of the SPIO nanoparticles (Fig. 2A) reveals that the magnetite nanoparticles have a spheroidal shape and are monodispersed. The average particle size estimated from TEM images is about 10.4 ±1.7 nm. TEM (Fig. 2B, C) and SEM (Fig. 2D) images of the SPIO@Au NPs indicate the formation of star-shaped nanoparticles with a size (tip to tip) of about 45 - 50 nm. (Fig. S3). The elemental composition of the SPIO@Au NPs was investigated by Energy Dispersive X-ray Spectroscopy (EDXS) analysis (Fig. 2E). The Au/Fe molar ratio was estimated to be about 13 confirming the presence of Fe_3O_4 phase in the nanoparticles. Unfortunately, Fe_3O_4 nanoparticles cannot be observed in TEM images, because gold coating prevents a deep electron penetration. Moreover, the higher diffraction intensity of Au and the strong overlap with the Fe_3O_4 features makes the magnetite phase identification in the Selected Area Electron Diffraction pattern the rather complex (Fig. S4). Microscopy analysis however did not reveals magnetic nanoparticles adsorbed outside of the SPIO@Au. This was also experimentally confirmed by acid etching experiments. To prove the continuity of the gold coating and rule out the presence of SPIO nanoparticles adsorbed on the gold surface, SPIO@Au nanoparticles were suspended in 1M HCL solution for 24 hrs.[19] HCl dissolve the iron oxide but not the metallic gold which protected the inner magnetic cores from dissolution, retaining the SPIO@Au magnetic and optical properties (Fig. S5). The chemical composition of the SPIO@Au after the HCL washing treatment was probed by linear scanning EDXS. EDXS line scan measurements show that Fe Kα line presents multiple peaks located in correspondence of the maximum of the Au Mα spectrum (Fig. S6).

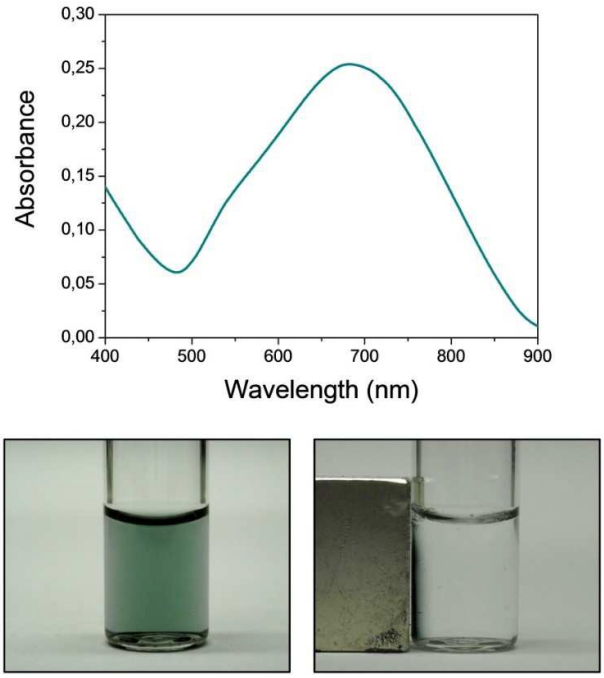

Fig 3. Up: Extinction spectrum of the SPIO@Au nanoparticles **Bottom:** Digital photographs of star shaped SPIO@Au suspension before (**left**) and after magnetic separation for 120 minutes (**right**).

This is a further confirm that the magnetic cores are located inside the gold nanostars. Scans of several SPIO@Au NPs from various batches also prove the successful SPIO incorporation on the SPIO@Au nanoparticles. Fig. 3 shows the UV-visible spectrum of SPIO@Au NPs in water. It presents a broad surface plasmon resonance band centered at about 695 nm and a weak shoulder at 530 nm. Kumar et al.[20] simulated the optical response of gold nanostars simulating the extinction spectrum of an object composed by a sphere and two cones. Simulated extinction spectra of star-shaped gold nanoparticles were composed by two principal components: a lower intensity peak located in the green – yellow part of the spectrum and a higher intensity component whose position strictly depends on the tip dimensions and shape. The first component was attributed to the modes localized on the central sphere, while the latter one was attributed to modes localized on the nanoparticles tips. In a similar way, the UV-vis absorption spectrum of the SPIO@Au NPs shows a small tail at 530 nm that can be assigned to the plasmon modes localized near the central sphere, and a main absorption peak at 700 nm

that can be attributed to the plasmon modes localized on the tips. SPIO@Au NPs can be easily separated from the solution by using commercial magnets as shown in Fig. 3. After about one hours, the nanoparticles were quantitatively deposited on the vial glass in proximity of the magnet while the solution results colourless. The magnetic character of the SPIO@Au NPs was clearly confirmed by the fast response of the particles to the external magnetic field. It is interesting to note that a 10 nm SPIO-PEG nanoparticles suspensions required almost two week for a complete magnetic separation in the same condition. The small dimensions of the magnetic cores (about 10 nm) limit the size of the magnetic domains, which results in a low magnetic moment value. SPIO@Au NPs required much less time to be separated probably due to the presence of multiple magnetic cores inside each star-shaped nanoparticle. The presence of several magnetic cores inside the same nanoparticle increases the magnetic moment of the material owing to the increase in the dimensions of the magnetic domains. SPIO@Au nanoparticles were characterized by NMR spectroscopy to test their relaxivity rate in water (Fig. S7). A linear relationship was obtained by plotting the reciprocal relaxation time and the concentration of iron in the sample. The value of the relaxivity for SPIO@Au obtained was 119 $sec^{-1}mM^{-1}$. This value is similar to that reported for iron oxide nanoparticles used in clinical imaging.[21] The high relaxivity rate of the SPIO@Au NPs opens the possibility to use these hybrid nanostructures as MRI contrast agents in *in vivo* applications. XPS analysis of the SPIO@Au NPs is reported in Fig. 4. A very low signal from iron was detected by XPS (Fig. 4A), whereas an intense doublet in the Au4f region corresponding to metallic gold (84 eV and 88 eV) was clearly observed (Fig. 4B). The Au/Fe atomic ratio obtained by XPS was about 21, a value lower to the one obtained by EDXS analysis. Taking into account that XPS is a surface sensitive technique with a sampling depth of about 5 nm, these results are expected to be a consequence of the incorporation of the magnetic nanoparticles inside the gold nanostars. The change in dimension and morphology of the SPIO@Au NPs were investigated as function of the total Au^{3+} concentration. At low $HAuCl_4$ concentration (1.0 mM), the average size of the resulting core–shell particles was about 50 nm with a broad absorption peak at around 695 nm. When the concentration of $HAuCl_4$ was increased up to 3.0 mM, the absorption peak experienced a redshift to 880 nm (Fig. 4C). This shift can be attributed to the change of the nanoparticles morphology and to the increase of the nanoparticles size. The average dimensions of the SPIO@Au particles increased to about 150 nm as reported in Fig. 4D. (Fig. S8). It was reported that gold may be reduced by the hydroxylamine only if metallic gold is already present in the suspension.[22, 23] In our previous work, we reported that hydroxylamine at strong basic condition can reduce the gold ions also in absence of external metallic gold.[24] In this paper the reduction process performed using the hydroxylamine was carried out in very basic conditions (pH 12). At this pH value the direct reduction of the gold chloride precursor is possible even in absence of preformed gold nuclei as in the seed-growth methods. As shown in Fig. 4D controlling the precursor concentration is possible to tune the dimensions of the synthesized nanoparticles.

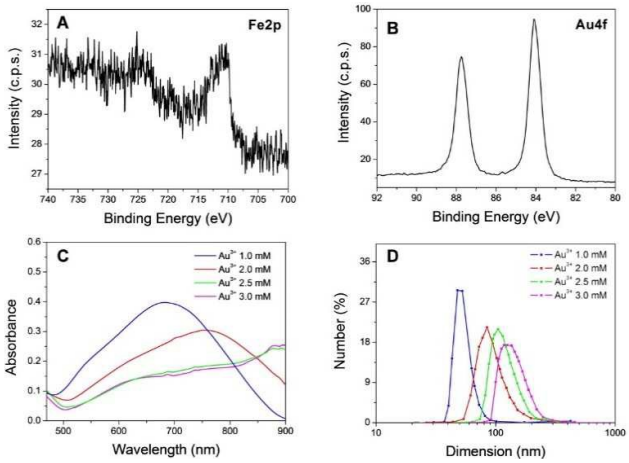

Fig. 4 A, B: Fe2p and Au4f core line XPS analysis of SPIO@Au nanoparticles. **C**: Uv-vis absorption spectroscopy of SPIO@Au nanoparticles synthetized with different Au^{3+} concentration **D**: Dynamic light scattering numerical size distribution of SPIO@Au nanoparticles synthetized with different Au^{3+} concentration.

It may be reasonably assumed that, during initial reduction of the gold precursor on the magnetic core, small gold nuclei are formed. The growth of these gold islands on the surface of the cores decrease the iron oxide nanoparticles water solubility since the PEG coating (which is principally responsible for the stability of the magnetic nanoparticles) is partially covered by gold. As a result, a certain number of magnetic cores aggregate, forming a nanoparticle clusters. At this point, the gold rapidly reduced on the magnetic nanoparticles clusters, covering the core and forming the star-shaped nanoparticle. For their possible use in biological applications, which require the use of a medium containing salts, proteins and other organic molecules, a further stabilization of the nanoparticles may be obtained by conjugation with various polymers containing functional groups. For the *in vitro* cell test measurement the SPIO@Au nanoparticles were functionalized by polyethylene glycol methyl ether thiol. The nanoparticles functionalized with PEG showed excellent stability both in high ionic strength solution and in biological media. The high scattering of the branched gold nanoparticles particularly in the red region of the spectrum was exploited for SPIO@Au localization in cells by laser scanning confocal microscopy analysis.[25] Conventional imaging techniques are normally performed by conjugating of fluorophores on the gold nanoparticles. These strategies however suffer from fluorescence quenching and require fluorescent probe immobilization of the nanoparticles surface.

Journal Name

ARTICLE

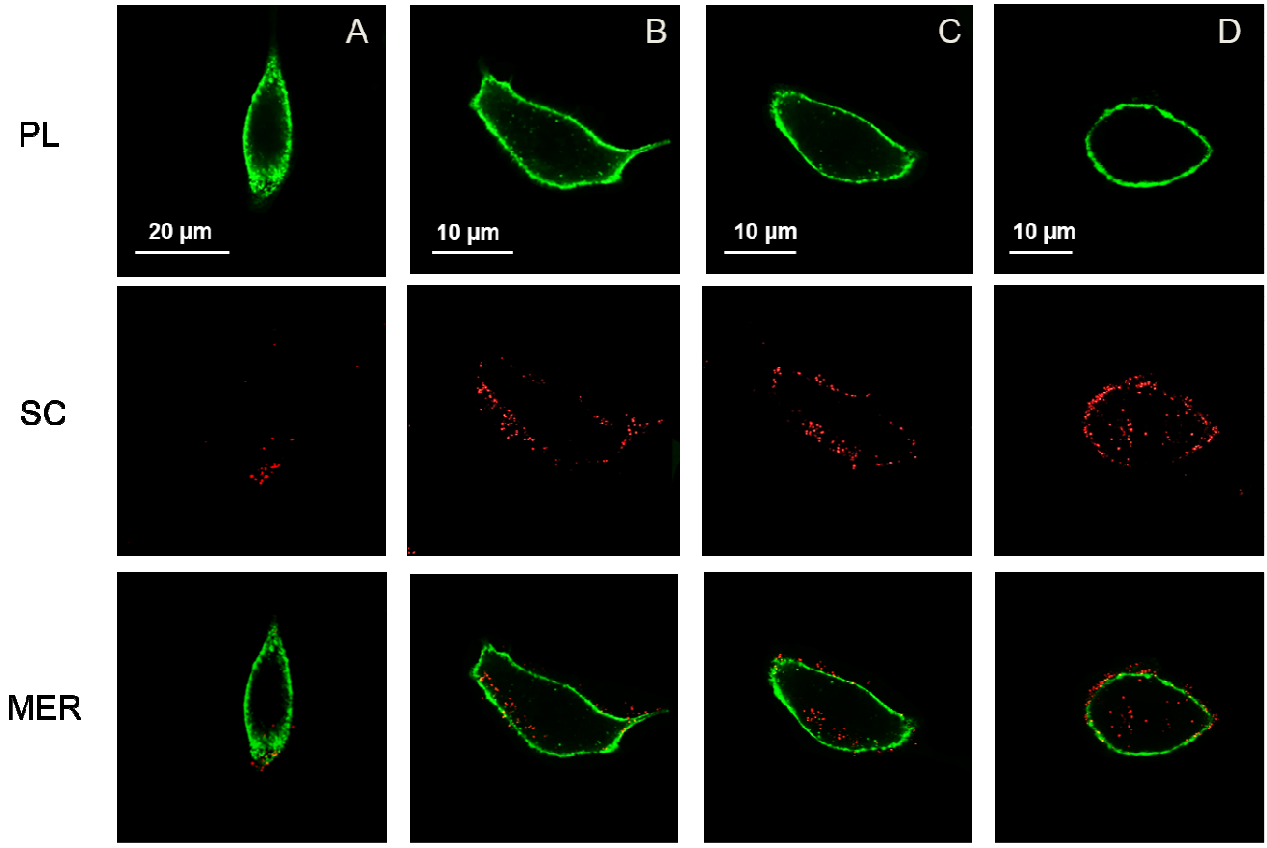

Fig. 5. Laser scanning confocal microscopy analysis of A549 cancer cell line incubated with SPIO@Au–PEG sample for 2 h. **PL** (WGA-Alexafluor 488 fluorescence), **SC** (gold nanoparticles) and **MER** (merge) images of four different cells.

On the contrary, the intense scattering of SPIO@Au NPs can be exploited for high resolution cell imaging, with no quenching issue and without the need of fluorescent probes.[26] A549 cancer cells were incubated with a 0.05 mg/ml SPIO@Au suspension for 2 h. Cellular membranes were then stained with WGA-Alexafluor 488 fluorescent probe and the localization of SPIO@Au was obtained by a 633 nm excitation laser source and a 620-650 nm band pass filter at very low laser power (0.5 mW). The low power and the very short acquisition times (about 1 minute) were chosen to limit possible heating of the SPIO@Au NP due to plasmonic effect. Negative controls were done by analyzing cells and cells incubated with WGA-Alexafluor 488 (data not show). For both controls no signal were detected at 633 nm indicating that the scattering can be unambiguously assigned to the SPIO@Au scattering.

The possibility to analyze simultaneously the membrane fluorescence and the nanoparticles scattering allow a precise determination of the nanoparticles position inside the cell. This information cannot be obtained by dark-field imaging, where the z-stacking is impossible and the advantage of fluorescent co-localization by CLSM cannot be exploited. Confocal microscopy analysis of A549 cancer cell line (Fig. 5) shows that a partial internalization of SPIO@Au is achieved already after 2 h of incubation. In Fig. 5A the red spots were localized mainly on the external membrane, while in Fig. 5 B, C a fraction of the nanoparticles was localized inside the cell in close vicinity to the membrane. In Fig. 5D nanoparticles are equally localized both on the external membrane and inside the cytosol. The dimensions of the red spots in the LSCM images are around 100 - 300 nm, bigger than that of a single

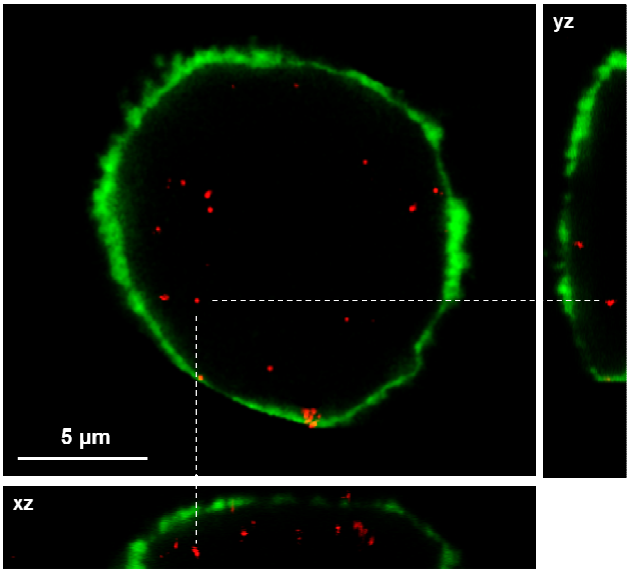

Fig. 6. Laser scanning confocal microscopy stacks top view and orthogonal views (xz and yz) analysis of A549 cancer cell line incubated with SPIO@Au–PEG for 2 h. SPIO@Au (red spots) and cell membrane (green). Optical images were collected every 0.7 µm beginning at the top of the cell and moving downward to the coverslip. Orthogonal images in the xz and yz planes indicate the SPIO@Au localization inside the cell.

SPIO@Au NP. These spots can be reasonably associated to multiple SPIO@Au NPs aggregates. The Au scattering signal was acquired with a narrow band pass (30 nm) to minimize the contribution from other fluorescent signals, like organelles autofluorescence and WGA Alexafluor. Furthermore, the precise control of the stage in the vertical axis allows a fine XY images acquisition. In Fig. 6, z-stack analysis of a single A549 cells is reported as well as vertical (yz) and horizontal (xz) planes of the 3D reconstruction

The images revealed that the Au spots were mainly localized in the cytoplasm as small clusters distributed overall the cell (Fig. S9). The formations of big nanoparticles clusters in the cytosol regions could indicate an endocytosis uptake pathway, as reported in the literature for similar nanoparticles.[27,28] Even though SPIO@Au NPs have demonstrated promising magnetic and optical properties much more efforts are required for the application of these nanoparticles in clinical studies. On the other hands, the combination of magnetic and optical properties present in a single nanoparticle can also be exploited to develop all-in-one functional nanoprobes for the isolation and recognition of biomarkers in blood and biological fluids. Gold surface functionalization with biomolecular targeting ligands will also allow simple conjugation to develop compact and efficient nanoprobes for molecular recognition and targeting. The magnetic properties can be exploited for the separation of the target from the biological media, while the plasmonic properties of the nanostars should provide molecular analysis capabilities

Conclusions

Magnetic–plasmonic nanoparticles composed by magnetic nanoparticles aggregates embedded in gold nanostars were produced by simple and low-cost chemical routes. Electron microscopy analyses confirm the formation of gold nanostructures around magnetic nuclei aggregates. The visible absorption spectroscopic analysis puts in evidences the presence of a broad absorption band in the red-near infrared region attributed to the plasmon resonance localized on the gold nanostars tips. Finally, confocal microscopy analysis demonstrates that SPIO@Au can penetrate the plasmatic membrane of A549 cell and be exploited as image contrast agent in *in vitro* cell experiments.

Acknowledgements

We thank the Laboratory of Biomolecular Sequence and Structure Analysis for Health (LaBSSAH) for the technical support.

Notes and references

1 G. Bao, S. Mitragotri S. Tong *Annu Rev Biomed Eng.* 2013, **15**, 253–282.
2 X. Jin, H. Li, S. Wang, N. Kong, H. Xu, Q. Fu, H. Gu, J. Ye *Nanoscale* 2014, **6**, 14360-70.
3 P. Quaresma, I. Osorio, G. Doria, P. A. Carvalho, A. Pereira,J. Langer, J. P. Araujo, I. Pastoriza-Santos, L. M. Liz-Marzan, R. Franco, P. V. Baptista and E. Pereira, *RSC Adv* 2014, **4**, 3659-3667.
4 E. M. Gindy, K. R. Prud'Homme *Expert. Opin. Drug Delivery* 2009, **6**, 865-878.
5 M. K. Yu, P. Park, S. Jon, *Theranostics.* 2012, **2**, 3–44.
6 Y. X. J. Wang *Quant. Imaging Med. Surg.* 2011, **1**, 35–40.
7 H. B. Na, I. C. Song, T. Hyeon *Adv. Mater.* 2009, **21**, 2133–2148.
8 A. Jasanoff *Curr. Opin. Neurobiol.* 2007, **17**, 593-600.
9 A. M. Smith, M. C. Mancini, S. M. Nie *Nat. Nanotech.* 2009, **4**, 710–711.
10 C. Wang, J. Irudayaraj *Small.* 2010, **6**, 283-9.
11 Y. Jin, C. Jia, S. W. Huang, M. O'Donnell, X. Gao, *Nat. Commun*. 2010, **1**, 41-48.
12 H. Yuan, C. G. Khoury, H. Hwang, C. M. Wilson, G. A. Grant, T. Vo-Dinh. *Nanotechnology*. 2012, **23**, 075102.
13 M. Qu, S. Mallidi, M. Mehrmohammadi, R. Truby, K. Homan, P. Joshi, Y. S. Chen, K. Sokolov, S. Emelianov *Biomed. Opt. Express.* 2011, **2**, 385–396.
14 H. M. Song, Q. Wei, Q. K. Ong, A. Wei, *ACS Nano* 2010, **4**, 5163–5173.
15 X. Miao, T. Wang, F. Chai, X. Zhang, C. Wang, W. Sun *Nanoscale* 2011, **3**, 1189-1194.
16 Q. Wei, H. M. Song, A. P. Leonov, J. A. Hale, D. Oh, Q. K. Ong, K. Ritchie, A. Wei *J. Am. Chem. Soc.* 2009, **131**, 9728-9734.
17 B. Dubertret, P. Skourides, D. J. Norris, V. Noireaux, A. H. Brivanlou, A. Libchaber *Science* 2002, **298**, 1759-1762.

18 NIST X-ray Photoelectron Spectroscopy Database http://srdata.nist.gov/xps/

19 H. Montazeri. A. Amani, H. R. Shahverdi, E. Haratifar, A. R. Shahverdi *J. Nanostruc. Chem.* 2013, **3**, 25.

20 P. S. Kumar, I. Pastoriza-Santos, B. Rodriguez-Gonzalez, F. J. Garcia de Abajo, L. M. Liz-Marzan *Nanotechnology* 2008, **19**, 01560.

21 Y. X. Wang *Quant. Imag. Med. Surg.* 2011, **1**, 35–40.

22 G. Stremsdoerfer, H. Perrot, J. R. Martin, P. J. Clechet, *Electrochem. Soc.* 1988, **135**, 2881-2885.

23 K. R. Brown, M. J. Natan *Langmuir* 1998, **14**, 726–728.

24 L. Minati, F. Benetti, A. Chiappini, G. Speranza *Colloids Surf., A Physicochem. Eng. Aspects* 2014, **441**, 623– 628.

25 L. Minati, V. Antonini, M. Dalla Serra, G. Speranza *Langmuir* 2012, **28**, 15900–15906.

26 L. Yuan, W. Wei, J. Li, Z. Sun, H. Wang, X. Zhang, Y. Chen *J. Nanopart. Res.* 2009, **11**, 1219–1225.

27 J. R. G. Navarro, D. Manchon, F. Lerouge, N. P. Blanchard, S. Marotte, Y. Leverrier, J. Marvel, F. Chaput, G. Micouin, A.-M. Gabudean, A. Mosset, E. Cottancin, P. L. Baldeck, K. Kamada, S. Parola, *Nanotechnology* 2012, **23**, 465602.

28 H. Yuan, C. G. Khoury, C. M. Wilson, G. A. Grant, A. J. Bennett T.Vo-Dinh *Nanomedicine* 2012, **8**, 1355–1363.

Graphical Abstract